INDUCTIVELY COUPLED POWER TRANSFER OF EVs USING DLCC TOPOLOGY

A Project Report

submitted by

AJSAL EK

in partial fulfilment of the requirements
for the award of the degree of

MASTER OF TECHNOLOGY

DEPARTMENT OF ELECTRICAL ENGINEERING
INDIAN INSTITUTE OF TECHNOLOGY MADRAS

JUNE 2021

CERTIFICATE

This is to certify that the thesis (or project report) titled **INDUCTIVELY COUPLED POWER TRANSFER OF EVs USING DLCC TOPOLOGY**, submitted by **AJSAL EK**, to the Indian Institute of Technology Madras, for the award of the degree of **Master of Technology**, is a bona fide record of the research work done by him (her) under my (our) supervision. The contents of this thesis (or project report), in full or in parts, have not been submitted to any other Institute or University for the award of any degree or diploma.

Place: Chennai

Date: 24th June 2021

Dr. Arun Karuppaswamy B
(Project Guide)
Assistant Professor
Dept. of Electrical Engineering
IIT Madras, 600 036

ACKNOWLEDGEMENTS

Foremost, I would like to express my sincere gratitude to my advisor Dr. Arun Karuppaswamy B for the continuous support for my M.Tech project. His guidance helped me in all the time of research and writing the thesis. In spite of his hectic schedule he was always approachable and took his time to discuss problems and give his advice and encouragement. I'am also grateful for suggesting proper literature throughout my study.

I'm grateful to Mr. Ravi Teja for clearing my doubts and constant support and encouragement. I also thank Mr. Bishal for helping me in simulations. He always found time to discuss the problems encountered during research.

I thank my batch mates Mr. Scaria Thomas, Mr. Bharath Reddy, Mr. Bhargava, Mr. Arun Kumar, Mr. Mohit Mangal, Bobby mathachan and Karthik for their support in writing the thesis. I also thank my seniors Mr. Arun Chithrabhanu and Mr. Harikrishnan for their support.

Finally I thank all my family members for their immense help and cooperation during toughtimes. This work could not have come to this stage without the support from them.

ABSTRACT

KEYWORDS: IWPT, DLCC, CC-CV charging, GSSA Modelling

IPT has several benefits than plugin charging in terms of greater convenience and safety. Battery used in most of the EV applications are Li-ion batteries due to its higher power density, long cycle life and better safety. To charge a Li-ion battery, we use constant current/constant voltage charging for better efficiency and protection. It is very difficult to ensure CC-CV charging without additional switches. In this project, we are implementing CC-CV charging by using load independent characteristics of an IPT system under ZPA condition. This project theoretically designs resonant tank for CC-CV mode at ZPA condition at two different resonant frequencies. Control system strategy is derived by developing small signal model of IPT system using GSSA method. The coil pad required for power transfer also is designed.

TABLE OF CONTENTS

Table of Contents (continued) **Page**

LIST OF TABLES

LIST OF FIGURES

ABBREVIATIONS

AWG	American Wire Gauge
CC	Constant Current
CPT	Capacitive Power Transfer
CV	Constant Voltage
DC	Direct Current
DLCC	Double sided LCC
EV	Electric Vehicle
GSSA	Generalised State Space Averaging
HEV	Hybrid Electric Vehicle
IC	Internal Combustion
ICNIRP	International Commission on Non-Ionizing Radiation Protection
ICPT	Inductively Coupled Power Transfer
IPT	Inductive Power Transfer
KVL	Kirchoff's Voltage Law
MIT	Massachusetts Institute of Technology
MPT	Microwave Power Transfer
PEV	Plugin Electric Vehicle
PI	Proportional Integral
PP	Parallel- Parallel
PS	Parallel -Series
PWM	Pulse Width Modulation
RF	Radio Frequency
RMS	Root Mean Square
SS	Series- Series
SP	Series- Parallel
WPT	Wireless Power Transfer
ZCS	Zero Current Switching
ZPA	Zero Phase Angle
ZVS	Zero Current Switching

NOTATION

English Symbols

Li	Lithium
Na	Sodium
M	Mutual inductance
n	Turns ratio
k	Coupling factor
L_1	Self inductance of primary coil
L_2	Self inductance of secondary coil
L_{1p}	Primary additional inductor
L_{1s}	Secondary additional inductor
C_{2p}	Primary parallel capacitor
C_{2s}	Secondary parallel capacitor
C_{1p}	Primary series capacitor
C_{1s}	Secondary series capacitor
f_{cc}	Frequency in CC mode
f_{cv}	Frequency in CV mode

Greek Symbols

β	Angle of conduction in degrees

CHAPTER 1

INTRODUCTION

1.1 History and Basics

Since the invention of internal combustion (IC) engines, petroleum products and flammable natural gases are extensively used in transportation. As the use of vehicles are increasing drastically, price of fuels which has a limited supply increased. Along with this, emission of poisonous green house gases also increased. This made industry and governments to focus more towards electric vehicles. Initially EVs were introduced as hybrid electric vehicles (HEV) which uses electric motors along with IC engines.

Earlier EVs were using Plug-in charging. EV will be parked in a charging station and get statically charged. There are two kinds of plugin charging based on the location of converters. They are on-board and off-board chargers. In on-board chargers, converters are placed inside PEV and in off-board chargers, converters are placed in charging station. Plugin charging requires charging cables and can be hazardous in rainy and snowy conditions due to its metal contacts.

Based on way of charging, wireless power transfer is of two types. Static and Dynamic charging. If vehicle is parked and getting charged, it is called static charging. If it is possible to charge while moving, it is called dynamic charging. Dynamic charging has the advantages like requirement of less weight battery, long range and time saving.

There are different kinds of static wireless charging methods such as microwave power transfer (MPT), capacitive power transfer (CPT), inductive power transfer (IPT) and inductively coupled power transfer (ICPT). Among these, ICPT can be used for dynamic charging as well.

Innovations in the field of wireless power transfer was of greater interest since Nikola Tesla invented it. The two factors limiting it was efficiency and transfer distance. Due to dominance in these two factors, magnetic resonance is preferred over other modes of wireless power transfer. Even though magnetic resonance was using since 1990's itself at 20 kHz range, it's transmission distance was not improved much. It was depending on the size of coil. So for getting reasonable transfer distance, it requires large sized coils. It was MIT who made a great leap in this by introducing resonance.

A WPT system consist of mainly 2 circuits. A primary and a secondary. Primary circuit produces power and send it to the receiver coil of secondary using a transmitting coil. Secondary consists the load which user has to power. An ideal WPT system should have a large air gap, high power and high efficiency.

In RF & Microwave systems, electromagnetic wave act as the means of propagating energy. We can transfer power in the range of meters but it have a great loss, very less efficiency and environmental impacts. MPT is referred as radiative (far field) technique and uses radio waves. In magnetic inductive and magnetic resonance coupling, variation of impedance has to be considered. But in MPT, since the transmitting and receiving coils are magnetically separable, impedance variation is not considered. It operates in the range of GHz. Power transferred is high but it is harmful to humans. It causes electromagnetic interference. Also cost incurred for MPT is high.

Capacitive power transfer method is a recent technology which uses capacitive coupling. It will have two metallic sheets which is coated with insulator at both primary and secondary side. In which a direct current is converted to a high frequency current using an inverter and an electric field is generated between primary and secondary and hence allow flow of current and power is transferred. The losses occurring in the metal sheets are very less compared to other methods. Therefore capacitive power transfer is more efficient and is good for EV charging. There is no need of ferrites for flux guiding. But capacitive coupling can be realised only for small transfer distance. Also it's cost is more than IPT. Capacitive method is not used for dynamic charging. It's advantages are high efficiency and it will not produce any interference with nearby communication

lines.

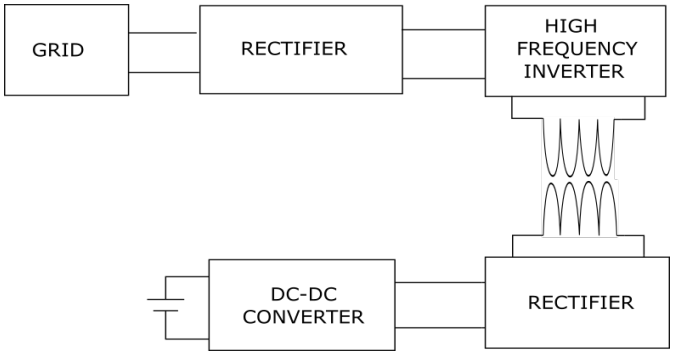

Fig. 1.1: Inductive Power Transfer

Inductive power transfer is based on electromagnetic induction.The problem with IPT is its poor efficiency. As the spacing between transmitter and receiver pads increases, leakage magnetic field of coupled inductor increases which reduces the efficiency because of it's loose coupling. In order to overcome this, resonant inductive power transfer which is also called ICPT was introduced by MIT in 2007 which can give a mid-range transfer distance, high efficiency and low interference. In ICPT method we use capacitors to compensate for the leakage magnetic field and hence increase efficiency. There are different compensation topologies to achieve this.

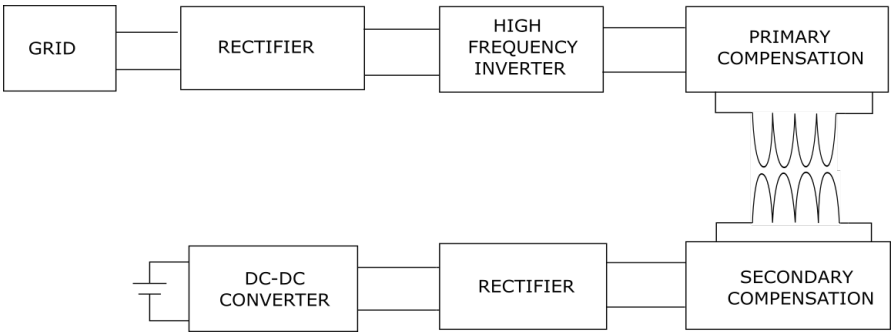

Fig. 1.2: Inductive Coupled Power Transfer

In IPT, grid ac voltage is converted to dc voltage using a rectifier and then converted to a high frequency ac voltage using an inverter which is required for wireless power transfer. This is passed through transmitting coil and a varying magnetic field is produced which in turn induces current in receiving coil. The received high frequency voltage is converted to DC using rectifier. This DC is used for battery charging. We can use a DC-DC converter in between rectifier and battery for controlling power flow.

1.2 Literature survey

(a) S.Y.Hui [1] presents a study on wireless charging of portable electronic products. It discusses the critical issues and technologies involved in planar wireless charging systems. It elaborates various international standards applicable for charging of portable devices.

(b) Dunkju Ahn et.al [2] presents WPT system for powering implantable biomedical devices with high efficiency and configured to maintain constant output voltage against coupling and loading variations.

(c) Ioana-Gabriela Sîrbu [3] analyse the three basic compensation topologies theoretically and experimentally. It derives expressions for transmitted power and efficiency for S-S, S-P, P-P tpologies and validate it experimentally. The study concluded that, among basic compensation topologies, Series-Parallel topology brings more advantages in terms of efficiency and transmitted power.

(d) Siqi Li [4] discusses the safety concerns in WPT charging. Even though WPT avoids electrocution danger from traditional contact charging method,In WPT, there is a high frequency magnetic field existing between the transmitting and receiving coils which cannot be shielded. This paper also discusses the ICNIRP standards for WPT.

(e) Tianze Kan [5] presents a new integration method for an electric vehicle wireless charging system for DLCC topology. Drawback of DLCC topology is it's large volume due to the compensated coils. The paper propose a method in which the five coupling effects are eliminated or minimised to a neglected level which simplifies the design and analysis.

(f) P. Srinivasa Rao NAYAK [6] compares series-parallel and dual-side LCC compensation topologies for wireless EV battery chargers. Misalignments (variation in mutual inductance) affects the electrical characteristics of these topologies. Analysis shows DLCC is better than S-P compensation in terms of misalignment tolerance, voltage and current stress on elements and efficiency.

(g) Bryan Esteban [7] compares two power supply architecture used for WPT, namely series LC (SLC) and LCL resonant inverter topologies. A 3 kW, 30 kHz charging system with a range of coupling (0.18-0.26) is developed. The study revealed that LCL topology maintin very high efficiency over it's full range of coupling and loading. Also LCL showed lesser capacitor voltage stress, lesser control complexity and good ZVS operation. But LCL is slightly costlier than SLC.

(h) Lu, J. et.al [8] compares S-S, S-P, S-SP, LCC-S, LCC-P and DLCC topologies. It derives condition for load independent voltage transfer characteristics with load independent ZPA. When considering the ESRs, it is found that DLCC topology is the most robust topology to obtain approximate constant voltage output and have the minimum error between experimental and designed values. So it can be used to achieve constant voltage with minimum power converter and control algorithm efforts.

1.3 Research objective

1. Understand the different compensation topologies used in ICWPT and select a proper topology.

2. Design a resonating tank in Constant cuurent- Constant voltage mode with ZPA condition. Also find the suitable resonance frequency for each mode.

3. Develop the small signal model of the designed ICWPT system and obtain the plant transfer functions.
4. Design a suitable coil pad required for wireless power transfer.
5. Design controllers required for Constant current-Constant voltage mode charging and verify its stability.
6. Verify the design using MATLAB SIMULINK and PSIM. Check responses under variable load conditions.

1.4 Organization of Thesis

Chapter 2 discusses the various batteries used in electric vehicles. It compares them on various aspects. The different charging methods for Li-ion battery is also presented with the relevant graphs.

Chapter 3 describes the compensation topologies used in wireless power transfer. Basic compensation topologies are compared in the perspective of constant current and constant voltage mode achievement with ZPA. Series-series compensation is analysed with relevant equations and figures.

Chapter 4 explains the DLCC topology which is used in this work. It derives the resonating frequency for constant current and constant voltage mode at ZPA. The methodology for design is presented. Resonant tank is designed using the proposed methodology.

Chapter 5 discusses the design of coil pad. High frequency effects such as proximity and skin effect are presented. Different coil structures are discussed. Analytical equations for circular and rectangular pads are given. Circular pad for the proposed system is designed. Litz wire to eliminate high frequency effects is also designed.

Chapter 6 deals with the Generalised state space averaging method. Some of the basic equations and models required for deriving state space is presentd. GSSA model of entire WPT system is given and required transfer functions are derived.

Chapter 7 presents the control strategy used in the design. Various control methods are introduced. Control design using frequency response is given. Simulation results from PSIM is provided for variable loads.

CHAPTER 2

BATTERIES AND CHARGING

2.1 Introduction

There are many kinds of batteries used in Electric vehicle applications. Since battery is an important factor which determines cost, range, safety, weight of vehicle and charging time of vehicle, it is very crucial to select proper battery and appropriate charging method. A study of comparison of different battery types is described in [9]. The various battery types available are Lithium-ion (Li-ion), Molten salt (Na-NiCl2), Nickel metal hydride (Ni-MH), Lithium Sulphur (Li-S) and Lead acid type.

Lead acid and Nickel metal hydride batteries were used in the starting days of EVs. But now they are considered outdated as a main source of energy as they have a very less specific energy of 34 Wh/Kg. Ni-MH batteries have a superior specific energy of 68 Wh/Kg and hence will use less space and will have less weight. But this type is also less used because of its low charging efficiency and self draining of charge. Also heat generation rate during fast charging and discharging is very high.

Most of the modern EVs use Li-ion batteries. Among various types of Li-ion batteries, electric vehicle industry is focused on variants which can provide higher longevity. Li-ion battery is almot one third of the weight of lead acid battery. Also it is three times powerful and have three times the cycle life. The specific energy of Li-ion battery is around 140+ Wh/Kg which is excellent. But the production cost of Li-ion batteries are three times that of Ni-MH batteries.

2.2 Common battery charging methods

The perfomance of a battery depends on the charging mode it is using. If a battery is charged using a high current, internal resistance of battery will increase which will increase the temperature and damage the battery in turn. If we are injecting a very less current in to battery, it will take much longer time to get charged which is not desirable. So selection of proper charging mode is very important for convenient use and life span of battery. Various charging methods are

2.2.1 Constant voltage charging

In this method, a constant voltage is applied across the battery. The advantage of this method is its simple circuitry and control design. As battery is getting charged, the charging current will get reduce. Battery will enter in to float charging when it is fully charged. But in the starting of charging, charging current will be very high because the battery voltage is very low . This high current will reduce the life span of battery.

2.2.2 Constant current charging

In this method, battery is charged with a fixed current. When battery is fully charged, charger turns into trickle charging to avoid overcharging and damaging. This method is generally faster compared to constant voltage charging. But care should be taken to avoid overcharging.

2.2.3 Pulsed charging

In this method, charging current is given as pulses as shown in Fig 2.1. Normally the pulse duration is 1 second and with short rest periods of 20 to 30 milli seconds to stabilise the reactions inside the cell.This will increase the life cycle of battery.

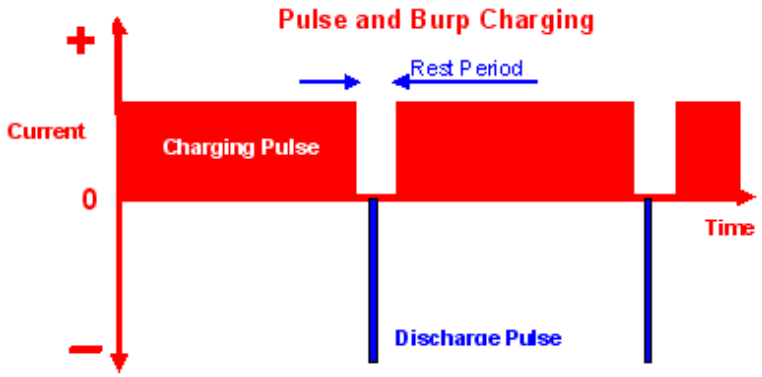

Fig. 2.1: Pulse and Burp charging

2.2.4 Burp charging

This method is also called negative pulse charging. During the charging rest period, it will apply discharging pulse, normally 2 to 3 times charging current for a duration of around 5 milliseconds. This will speed up the stabilisation process of electrolytes than pulsed charging.

2.2.5 CC/CV charging

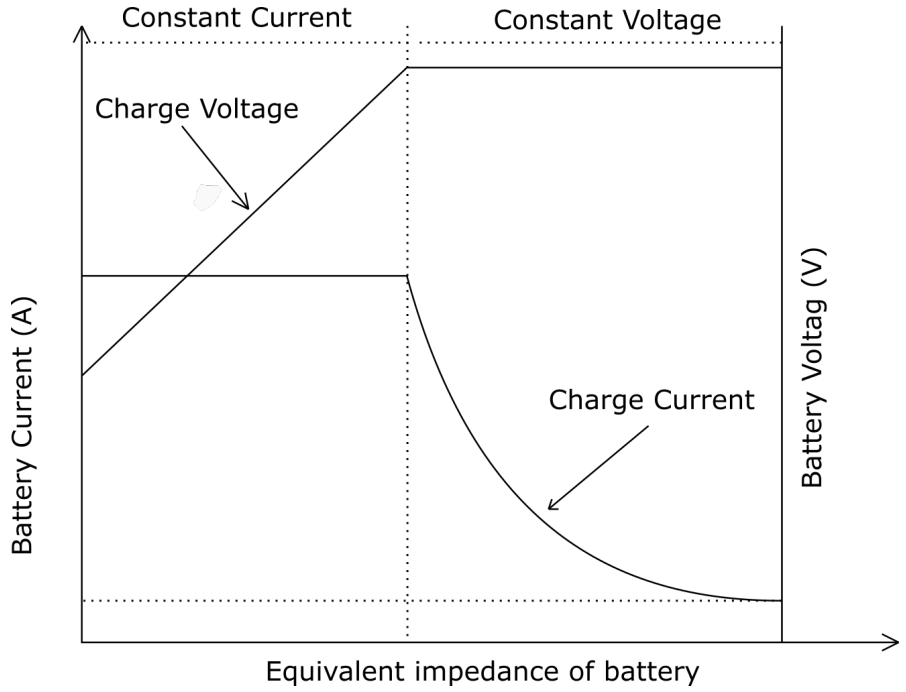

Fig. 2.2: CC-CV charging mode

Constant voltage and constant charging methods have their own disadvantages. To overcome these shortcomings, a constant current followed by constant voltage charging method is widely used. This will reduce the problem of overcharging and reduce the high initial charging current. Charging time also will get reduced.

2.2.6 Conclusion

Among the various types of batteries available, electric vehicle industry uses Li-ion battery due to its high energy density and can provide a good range for vehicles. Li-ion battery uses CC/CV charging method for attaining good life span and better charging.

CHAPTER 3

COMPENSATION TOPOLOGIES

3.1 Introduction

One of the objective of our design must be to minimize volt-ampere characteristics of source and increase transmission power. For this, leakage inductance has to decrease. The primary resonance cancels leakage inductance which will ensure operation near unity power factor with secondary also operating at same resonant frequency. The tuning of capacitor is done in such a way that input voltage and current are in-phase at certain coupling and load condition which is called Zero Phase Angle (ZPA) method. Also these combinations will act as a good harmonic filter which passes only fundamental component of input voltage.

Depending on how the capacitors are connected to the coils, there are four basic compensation topologies, which are series-series (SS), series-parallel (SP), parallel-series (PS) and parallel-parallel (PP) as shown in Fig 3.1. Each topolgy has its own advantages and disadvantages. Based on application we have to choose the compensation. They shows different trend towards factors like misalignment tolerance and CC/CV operation. For achieving merits of each topology, modified or combination of four basic topologies are used. But it will make the system more complex and costlier. Design of control will be more difficult in such cases. The various modified topologies are SP-S, LCL-S, LCC-LCC (Double sided LCC), LC-LC, etc. The analysis of a basic topology will be discussed in detail in this chapter.

3.2 Fundamental Analysis of S-S compensation

For better analysis of loosely coupled transformer, we use two equivalent models as shown in Fig 3.2 and 3.5. a) T model and b) M model. M is the mutual inductance, L_1

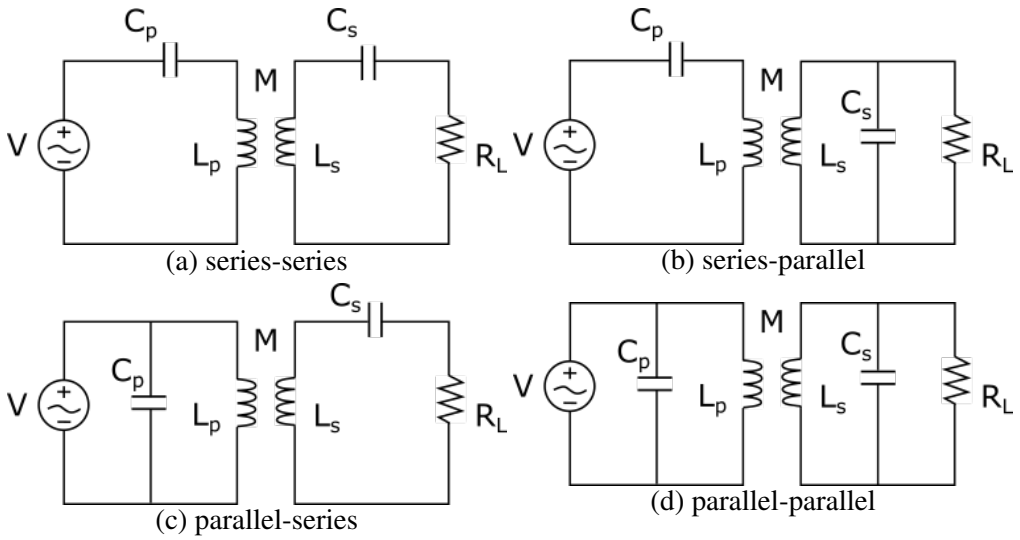

Fig. 3.1: Basic compensation topologies

and L_2 are the primary and secondary self inductances. L_{l1} and L_{l2} are the primary and secondary leakage inductances.The fundamental equations are.

$$M = nL_m \tag{3.1}$$

$$L_1 = L_{l1} + L_m = L_{l1} + \frac{M}{n} \tag{3.2}$$

$$L_2 = L_{l2} + n^2 L_m = L_{l2} + nM \tag{3.3}$$

$$k = \frac{M}{\sqrt{L_1 L_2}} \tag{3.4}$$

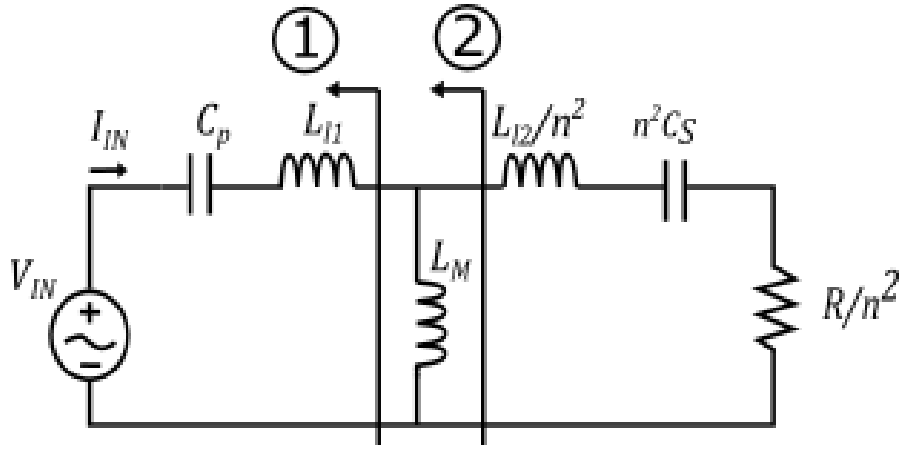

Fig. 3.2: Equivalent T Model of SS topology

Let the resonating frequency is f_{sw}. C_p and C_s are the primary and secondary

compensating series capacitors respectively. If resonating frequency is chosen such that

$$f_{sw} = \frac{1}{2\pi\sqrt{L_{l1}C_p}} \tag{3.5}$$

$$f_{sw} = \frac{1}{2\pi\sqrt{L_{l2}C_s}} \tag{3.6}$$

This is shown by condition 1 in Fig.3.2. Then circuit shown in Fig.3.2 will simplify in to Fig.3.3. Then the output voltage will be $V_o = nV_{in}$ which is load independent which means, we will get a constant voltage output. For ensuring ZPA condition, impedance seen by input (Z_{in}) has to be found at this frequency. From Fig 3.3, it is clear that Z_{in} is inductive due to the presence of L_m. So CV mode operation at ZPA condition is not possible using S-S compensation. For operation in ZPA condition, L_m has to be compensated using an additional parallel capacitance across it.

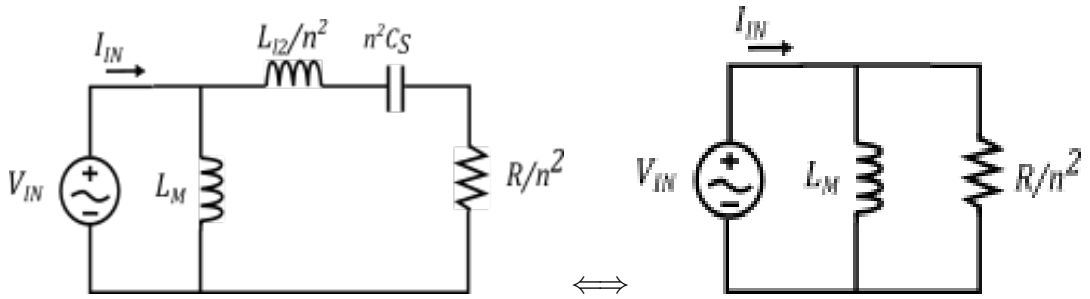

Fig. 3.3: Reduced Model at condition 3.5

If we operate the circuit at a frequency f_{sw} as in Eq 3.7

$$f_{sw} = \frac{1}{2\pi\sqrt{(L_{l1} + L_m)C_p}} = \frac{1}{2\pi\sqrt{L_pC_p}} \tag{3.7}$$

Then Fig 3.2 will reduce into Fig 3.4. Then we will get a current source with an output current $i_o = \frac{v_{in}}{\omega L_m}$ which is load independent as shown in Fig 3.4, which means if we are operating the circuit in resonating frequency as in Eqn 3.7 , we will get a constant current output. For achieving ZPA condition, Z_{in} has to be found. For that we can use M model as shown in Fig 3.5.

$$Z_p = j\omega L_p + \frac{1}{j\omega C_p} \quad ; \quad Z_s = j\omega L_s + \frac{1}{j\omega C_s} + R \tag{3.8}$$

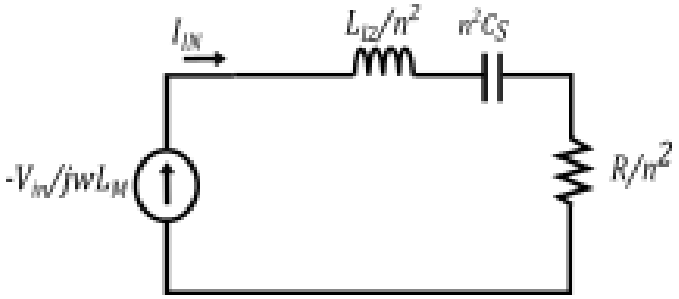

Fig. 3.4: Reduced model at condition 3.7

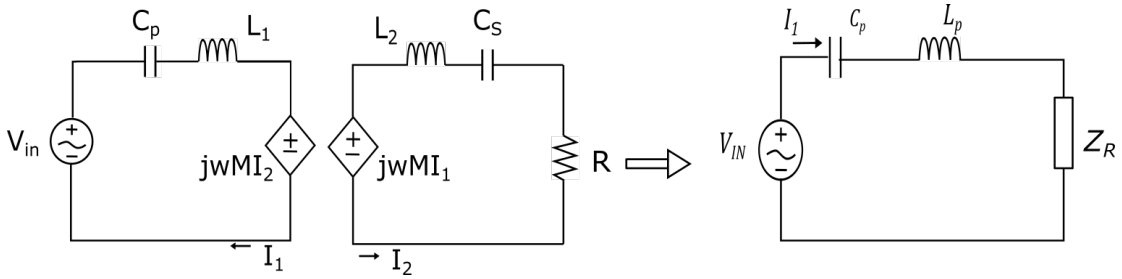

Fig. 3.5: M model of SS topology

$$Z_{in} = \frac{V_{in}}{I_p} = Z_p + Z_R \quad ; \quad Z_R = \frac{j\omega M I_s}{I_p} = \frac{\omega^2 M^2}{Z_s} \tag{3.9}$$

If we are choosing C_s such as it will compensate for L_s, then Z_{in} will be purely resistive. So it is clear that SS compensation can be used to operate the circuit in constant current mode under ZPA.

If we follow similar approach to all other basic compensations, we can see that none of them give ZPA operation in both CC and CV operation. So we will choose modified topologies which will give us more degrees of freedom for design. The summary of basic compensation topologies is given in Table 3.1.

3.2.1 Need for modified topologies

There are some topologies which use mix of basic compensation to achieve CC-CV operation with the help of additional switches which decreases the reliability of the system. So a better method will be, deriving condition to operate in constant current and constant voltage at ZPA condition and use PWM for controlling output current or voltage. Basic compensation topologies cannot provide CC-CV operation with ZPA as we

Compensation circuits	Conditions	Load independent conditions	ZPA
SS	$\omega = \frac{1}{\sqrt{L_1 C_p}} = \frac{1}{\sqrt{L_2 C_s}}$	$i_o = \frac{v_{in}}{\omega M}$	**Yes**
	$\omega = \frac{1}{\sqrt{L_{l1} C_p}} = \frac{1}{\sqrt{L_{l2} C_s}}$	$v_o = n v_{in}$	**No**
SP	$\omega = \frac{1}{\sqrt{(L_1 - \frac{M^2}{L_2}) C_p}} = \frac{1}{\sqrt{L_2 C_s}}$	$v_o = \frac{L_2 v_{in}}{M}$	**Yes**
	$\omega = \frac{1}{\sqrt{L_{l1} C_p}} = \frac{1}{\sqrt{L_{l2} C_s}}$	$i_o = \frac{n v_{in}}{\omega L_{l2}}$	**No**
PS with Lx	$\omega = \frac{1}{\sqrt{L_1 C_p}} = \frac{1}{\sqrt{L_2 C_s}}$ and $L_x = L_1$	$v_o = \frac{M v_{in}}{L_1}$	**Yes**
PP with Lx	$\omega = \frac{1}{\sqrt{(L_1 - \frac{M^2}{L_2}) C_p}} = \frac{1}{\sqrt{L_2 C_s}}$ and $L_x = L_1 - \frac{M^2}{C_s}$	$i_o = \frac{M v_{in}}{\omega (L_p - \frac{M^2}{L_2}) L_2}$	**Yes**

Table 3.1: Characteristics of IPT circuits with basic compensations

discussed in this chapter. So we use modified topologies which will give more degrees of freedom for design.Detailed discussion on Double sided LCC (DLCC) compensation is given in next chapter.

3.3 Conclusion

In this chapter, the necessity of compensation is discussed. Also the various basic compensation topologies are introduced. A basic analysis of series-series compensation is discussed. Condition for constant current mode at ZPA is derived. It is found that Basic compensation topologies cannot be used for CC-CV charging without additional components.

CHAPTER 4

DLCC topology

4.1 Introduction

In this topology design, we will ensure both CC and CV mode of operation at ZPA condition at two different resonant frequencies. Load independent operating condition of both constant current and constant voltage is derived. This design has the following advantages.

(a) In many of the IPT chargers, resonant converter will operate in maximum efficiency frequency and an additional DC-DC back-end converter between resonant tank and battery is used to ensure CC-CV operation. This will increase the cost, complexity and reduce the reliability and efficiency. In this design, CC-CV operation is guaranteed without back-end converter.

(b) Some design approaches uses help of additional switches to shift from CC to CV mode. They design CC operation using one compensation and CV operation in a different compensation.CC-CV transition is done with the help of additional switches. Such scheme is called Hybrid compensation. But it will require more switches and its driver circuits which will increase cost and reduce reliability.

(c) Perfect ZPA condition in both CC and CV operation.

The DLCC topology is given in Fig.4.1. The primary compensation consist of an resonant inductor(L_{1p}) and two resonant capacitors (C_{1p} and C_{2p}). C_{1p} is in series and C_{2p} is in parallel with primary . Secondary compensation is also arranged in a similar way(L_{1s},C_{1s} and C_{2s}). Let L_1 and L_2 are the self inductances. L_{rp} and L_{rs} leakage inductances and L_m and M are the magnetising and mutual inductance respectively. Coupling coefficient k can be expressed as

$$k = \frac{M}{\sqrt{(L_m + L_{rp})(L_m + L_{rs})}} = \frac{M}{\sqrt{L_1 L_2}} \tag{4.1}$$

$$L_{rp} = (1-k)L_1; L_{rs} = (1-k)L_2 \tag{4.2}$$

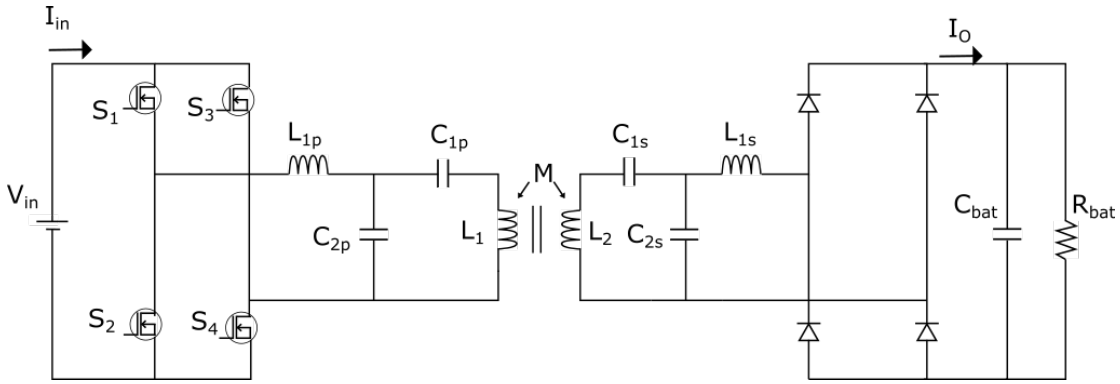

Fig. 4.1: DLCC Topology

Let V_{in}, V_o, I_o represent DC link voltage , output voltage and output current.

4.2 CC mode with ZPA condition

From Fig 4.2, using Kirchoff's voltage law (KVL) equation in primary side,

$$V_{in} = \left(j\omega L_{1p} - j\frac{1}{\omega C_{2p}} \right) I_{in} - \frac{1}{j\omega C_{2p}} I_1 \tag{4.3}$$

KVL in secondary gives

$$j\omega M I_1 = j\left(\omega L_2 - \frac{1}{\omega C_{2p}} - \frac{1}{\omega C_{2s}} \right) I_2 + j\frac{1}{\omega C_{2s}} I_o \tag{4.4}$$

From these equations, I_o can be made only in terms of input voltage V_{in} only if

$$\omega_{cc} L_{1p} - \frac{1}{\omega_{cc} C_{2p}} = 0 \tag{4.5}$$

$$j(\omega_{cc} L_2 - \frac{1}{\omega_{cc} C_{1s}} - \frac{1}{\omega_{cc} C_{2s}}) = 0 \tag{4.6}$$

where ω_{cc} represent constant current resonating frequency. Then output current is given by

$$I_o = \frac{\omega_{cc}^3 C_{2s} C_{2p} M V_{in}}{j} = \frac{M V_{in}}{j\omega_{cc} L_{1p} L_{1s}} \tag{4.7}$$

From Eqn 4.7 , it is clear that, output current depends only on input voltage, operat-

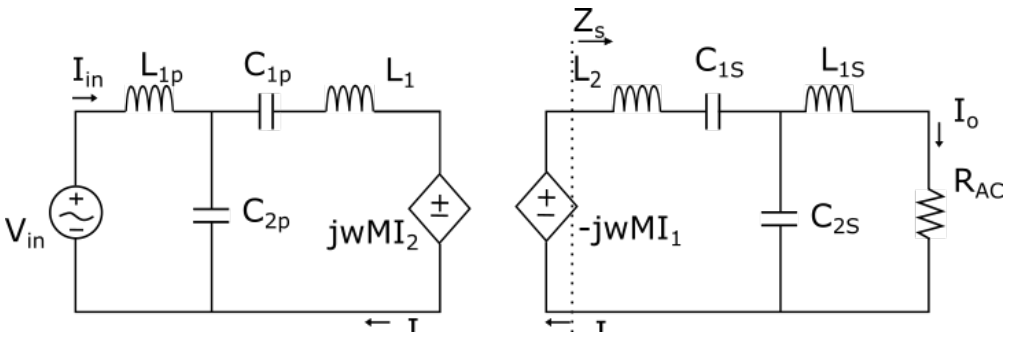

Fig. 4.2: M model of double sided LCC compensation topology

ing frequency and compensation parameters which implies that constant current mode is achieved. For obtaining ZPA condition, input impedance at this frequency has to be found. Secondary impedance Z_s can be derived as

$$\begin{aligned} Z_s &= j(\omega L_2 - \frac{1}{\omega C_{1s}} - \frac{1}{\omega C_{2s}})//(j\omega L_{1s} + R_{AC}) \\ &= \frac{1}{\omega^2 R_{AC} C_{2s}^2 + j\omega C_{2s}(\omega^2 L_{1s} C_{2s} - 1)} \end{aligned} \tag{4.8}$$

The reflected impedance of secondary seen by primary is given by

$$Z_R = \frac{j\omega M I_2}{I_1} = \frac{-(\omega M)^2}{Z_s} \tag{4.9}$$

From Fig 4.18, Input impedance Z_{in} is given by

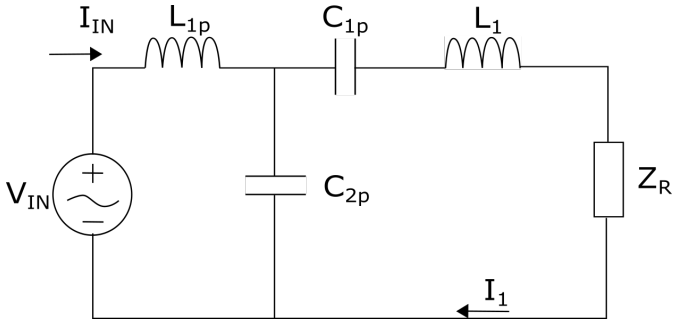

Fig. 4.3: Simplified M model of DLCC

$$Z_{in} = j(\omega L_{1p} - \frac{1}{\omega C_{2p}}) + \frac{1}{\omega^2 C_{2p}^2 [Z_N - \frac{(\omega M)^2}{Z_s}]} \tag{4.10}$$

where $Z_N = j(\omega L_1 - \frac{1}{\omega C_{1p}} - \frac{1}{\omega C_{2p}})$. In-order to achieve ZPA condition , we have to

make imaginary part of Z_{in} zero. For that,

$$\omega_{cc}^2 L_{1s} C_{2s} - 1 = 0 \tag{4.11}$$

$$\omega_{cc} L_1 - \frac{1}{\omega_{cc} C_{1p}} - \frac{1}{\omega_{cc} C_{2p}} = 0 \tag{4.12}$$

. Therefore equations 4.5, 4.6, 4.11, 4.12 has to be satisfied for achieving CC mode at ZPA condition.

4.3 CV mode with ZPA condition

For simplicity of design and easy calculation, the resonating tank parameters are chosen as

$$\begin{aligned} L_{1p} &= L_{1s} \\ C_{1p} &= C_{1s} \\ C_{2p} &= C_{2s} \end{aligned} \tag{4.13}$$

For an easy analysis Fig 4.2 is simplified into Fig 4.4 (a) and it is further simplified into 4.4 (b) using Y$-\Delta$ transformation. In Fig 4.4,

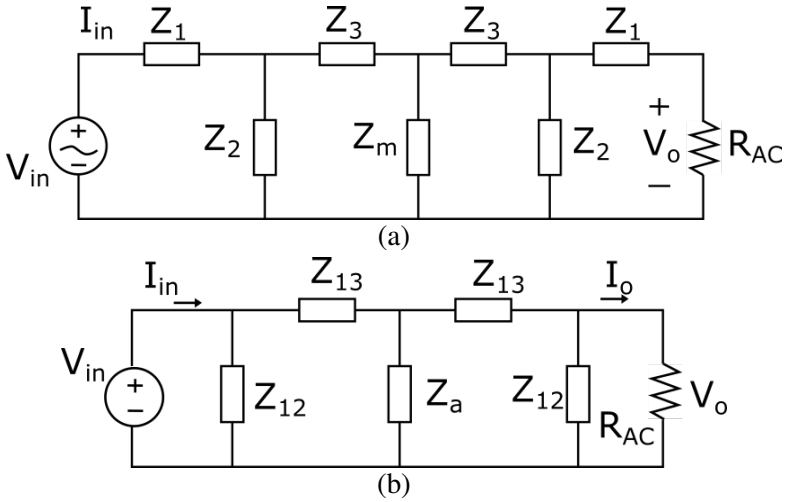

Fig. 4.4: a) Simplified equivalent circuit of DLCC b) Further simplified by applying Y-Δ transformation

$$
\begin{aligned}
Z_m &= j\omega L_m \\
Z_1 &= j\omega L_{1p} = j\omega L_{1s} \\
Z_2 &= \frac{1}{j\omega C_{2p}} = \frac{1}{j\omega C_{2s}} \\
Z_3 &= \frac{1}{j\omega C_{1p}} + j\omega L_{rp} = \frac{1}{j\omega C_{1s}} + j\omega L_{rs}
\end{aligned}
\tag{4.14}
$$

$$
\begin{aligned}
G_v &= \frac{V_o}{V_{in}} \\
&= \left| \frac{Z_a(Z_{12}||R_{AC})}{(Z_{12}||R_{AC})(Z_{13}+Z_a)+Z_{13}(Z_{13}+Z_a)+Z_{13}Z_a} \right| \\
&= \left| \frac{Z_a}{Z_{13}+Z_a+\frac{Z_{13}(Z_{13}+2Z_a)}{Z_{12}}} + \frac{Z_{13}(Z_{13}+2Z_a)}{R_{AC}} \right|
\end{aligned}
\tag{4.15}
$$

where

$$
\begin{aligned}
Z_{12} &= Z_1 + Z_2 + \frac{Z_1 Z_2}{Z_3} \\
Z_{13} &= Z_1 + Z_2 + \frac{Z_1 Z_3}{Z_2} \\
Z_{23} &= Z_2 + Z_3 + \frac{Z_2 Z_3}{Z_1} \\
Z_a &= \frac{Z_m Z_{23}}{2Z_m + Z_{23}}
\end{aligned}
\tag{4.16}
$$

For making voltage gain independent of load resistance R_{AC},

$$
Z_{13}(\omega_{cv})[(Z_{13}(\omega_{cv}) + 2Z_a(\omega_{cv})] = 0 \tag{4.17}
$$

$Z_{13} = 0$ condition cannot be satisfied as it results in to a condition in which power cannot be transferred. So we are taking the condition

$$
Z_{13}(Z_{13} + 2Z_a) = 0 \tag{4.18}
$$

For achieving ZPA, Z_{in} at condition 4.18 has to be found. Z_{in} derivation is complex and is discussed in [10]. The condition for ZPA at CV mode is

$$
2Z_a(\omega_{cv}) - Z_{12}(\omega_{cv}) = 0 \tag{4.19}
$$

If we are satisfying both Eqn. 4.18 and 4.19, constant voltage at ZPA is achieved.

DLCC compensation parameters are designed satisfying all these 7 equations. It will require some iterations by taking CC frequency as 68 kHz to get the exact values.

4.4 Proposed system

CC-CV charging system is developed for a Li-ion battery without using on board DC-DC converter. The specifications of proposed system is given in Table 4.1

P_0	Power rating	6.6 kW
V_{in}	Input Voltage	400 V [DC]
V_0	Output Voltage	250-420 [V]
I_0	Output current	15.7 [A]

Table 4.1: Specification of IPT charger

From the design methodology descried in the previous section the resonant DLCC compensation tank is designed. The resonant tank parameters are given in Table 4.2

L_1	Self inductance of primary coil	$218.3\ \mu$H
L_2	Self inductance of secondary coil	$218.3\ \mu$H
M	Magnetizing inductance	$57.3\ \mu$H
L_{1p}	Primary additional inductor	$53.1\ \mu$H
L_{1s}	Secondary additional inductor	$53.1\ \mu$H
C_{2p}	Primary parallel capacitor	102 nF
C_{2s}	Secondary parallel capacitor	102 nF
C_{1p}	Primary series capacitor	33 nF
C_{1s}	Secondary series capacitor	33 nF
f_{cc}	Frequency in CC Mode	68 kHz
f_{cv}	Frequency in CV Mode	79.1 kHz

Table 4.2: Resonant tank parameters

4.5 Conclusion

DLCC resonating tank is designed to achieve Constant current-Constant voltage mode charging without use of an additional back-end converter. The equations derived from

the required condition is solved using iteration. Constant current and constant voltage is achieved by making output current and output voltage independent of load. Design ensures Zero Phase Angle condition in both CC and CV modes.

CHAPTER 5

COIL DESIGN

5.1 Introduction

The transmitting and receiving coils in a WPT is it's backbone. The two coils are coupled through a fairly high air gap which causes very less mutual inductance (loosely coupled) and the coupling factor will be in the range of (0.1-0.3). The geometry and materials of this pair of coils are crucial for determining the magnetic field of the WPT and it's efficiency. Also the electrical parameters of the coils will determine the configuration of the compensation networks.

In a complex design process, both economical and electrical factors should be considered while determining geometry and configuration of coils. Use of certain materials which is required for high frequency operation will increase the cost of coil. So length of cables and size of ferromagnetic elements should be taken carefully. Also the coil geometry and size are important for self inductance, their quality factor and the mutual inductance.

The mutual inductance between the coils will change when their relative positions are changed. This will cause change in power transferred and efficiency of the system. So our coil geometry should withstand such changes which is termed as misalignment tolerance. There can be horizontal, vertical, horizontal plus vertical or angular misalignment. angular misalignment is not common in EV wireless chargers.

Complex coil structures incorporates magnetic and metallic materials to control the propagation of the magnetic field involved in the WPT. Ferromagnetic material help to guide the magnetic field to the area of interest where as the metallic elements prevent it's propagation into protected zones. The inclusion of this materials will change electrical parameters of coils. Also these changes cannot be easily estimated by equations. Finite

element analysis software which require high computational ability should be used to characterise them.

5.2 High frequency effects

When dealing with high frequency components, there are some other effects which have to be considered. They are proximity and skin effect.

5.2.1 Proximity effect

Proximity effect is the tendency for current to flow in other undesirable patterns, loops, or concentrated distributions due to the presence of magnetic fields generated by nearby conductors. In fact, when another conductor is brought into proximity to one or more other nearby conductors, such as within a closely wound coil of wire, the distribution of current within the conductor will be constrained to smaller regions. Field intensity is no longer uniform around each conductor surface. The resulting current crowding is termed as the 'proximity effect' and increases with the frequency. This current crowding gives an increase in the effective resistance which results in higher power losses in the wire.

In transformers and inductors, proximity-effect losses typically dominate over skin-effect losses. In Litz-wire windings, proximity effect may be further divided into internal proximity effect (the effect of other currents within the bundle) and external proximity effect (the effect of current in other bundles). The actual losses in one strand of a Litz bundle are simply a result of the total external field, due to the currents in all the other strands present.

5.2.2 Skin effect

When a wire is carrying a DC current, the current is distributed uniformly over all the effective area of the wire. This current distribution is non-uniform when the wire

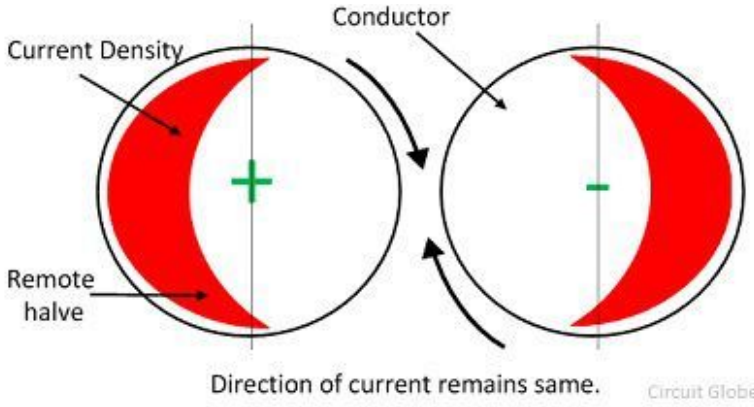

Fig. 5.1: Change in current concentration due to proximity effect

is carrying an alternating current, as the current intensity and the magnetic field in a conductor change and results in a phenomenon known as 'skin effect'. The skin effect is the restriction of the flow of alternating current to the surface of a conductor. This restriction is caused by the alternating magnetic field that the current itself generates within the conductor.

The current flowing in the conductor generates a magnetic field around it. This field in turn creates circulating currents in the wire. These currents are opposite to the main current flow in the centre of the conductor and add to the main current closer to the surface of the wire. The result is that more net current is flowing closer to the surface of the conductor, and eventually an increase in the effective resistance of the conductor due to the reduced cross sectional area for current flow. This area of current flow between the outer surface and a level of the conductor diameter is called the 'skin depth'. The skin depth is thus defined as the depth below the surface of the conductor at which the current density has fallen to 1/e(about 0.37) of J_S. Typically, it is well approximated as:

$$\delta = \sqrt{\frac{2\rho}{\omega\mu}} \tag{5.1}$$

where ρ is the resistivity of the conductor, ω is the angular frequency of the current, and $\mu = \mu_r\mu_0$ is the absolute magnetic permeability of the conductor.

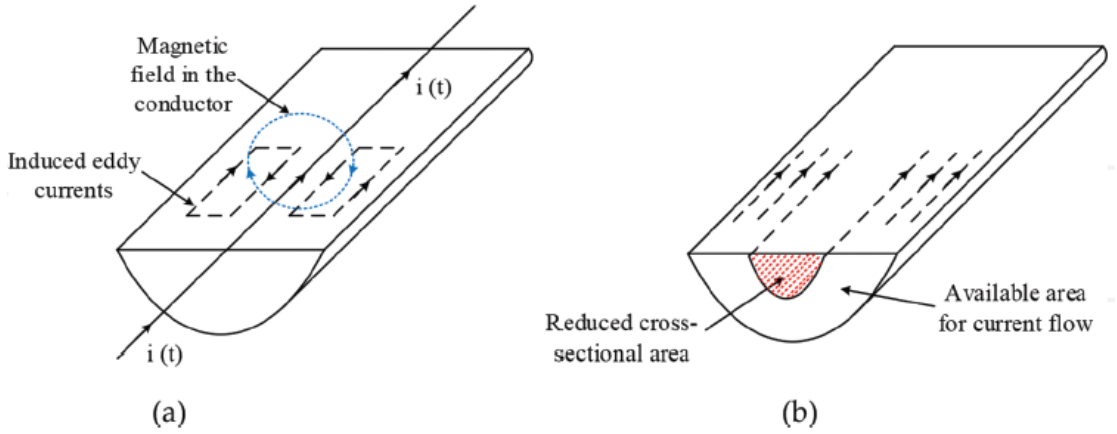

Fig. 5.2: Impact of skin effect on the coil ESR: (a) generated eddy currents and (b) reduced cross-sectional area due to skin effect.

5.3 Pad topologies

There are different types of coil structures available. Polar and Non-polar pads. They are classified according to the geometry of the coil. They are a) Double D (**DD**) b) DD quadrature (**DDQ**), c) Bipolar d) Circular e) Rectangular. The first three are given in Fig 5.3.

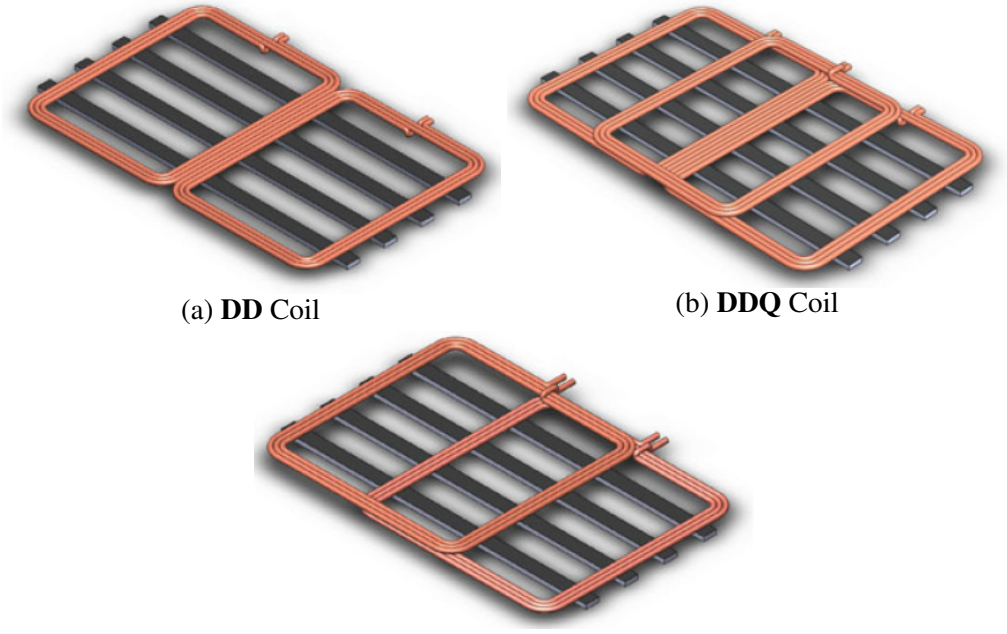

(a) **DD** Coil

(b) **DDQ** Coil

(c) Bipolar Coil

Fig. 5.3: **DD**,**DDQ** and Bipolar coils

5.4 Analytical design of Coils

Since we are operating in the range of 80 kHz, increase in resistance of the wire due to eddy currents needs to be considered which is caused by skin effect and proximity effect. In order to reduce these effects we use braided enamelled conductors known as Litz wire.

A Litz wire consists of many thin strands, each individually insulated, wound into a wire. Each strand is no thicker than the skin depth, which ensures an efficient use of the conductive area.The strands are then woven together so that the location of each strand alternates between the centre of the wire and the edge of the wire. This ensures that the proximity effect will affect each strand the same, and thus carry the same current.

5.4.1 Design of Litz wire

In a Litz wire design, number of strands and overall gauge of the wire is the parameters to be calculated.

(a) For calculating the overall gauge of the wire, allowed current density of the wire have to be decided. For proper cooling in this power range, generally it is chosen as 2 to 6 A/mm^2. Then the gauge can be chosen from the current density and maximum current flowing through the coil considering safety margin also.

$$Area\ of\ crossection\ of\ wire = \frac{current}{current\ density} \tag{5.2}$$

Here the design is done by taking peak current of 27 A. A maximum current density of 5 A/mm^2 is chosen. Then from Eq 5.2 area is calculated as 5.4 mm^2. According to American wire gauge (AWG), AWG 9 is selected whose diameter is 2.9064 mm and have an area of 6.6342 mm^2.

(b) For calculating number of strands, skin depth have to be calculated using Eq. (5.1). Where ρ is the resistivity of the conductor which is equal to $1.72 \times 10^{-7}\Omega - m$, ω is the angular frequency of the current, which is $2\pi \times 68000$ rad/s and $\mu = \mu_r\mu_0$ is the absolute magnetic permeability of the conductor, which is equal to $4\pi \times 10^{-7}$ H/m. Skin depth calculated is 0.240 mm. The diameter of a selected strand should be less than the skin depth. A good design uses a strand diameter smaller than the skin depth by a factor of 4 or more. Therefore, a strand of 42 AWG (0.0633mm) diameter is selected. The number of strands can then be given

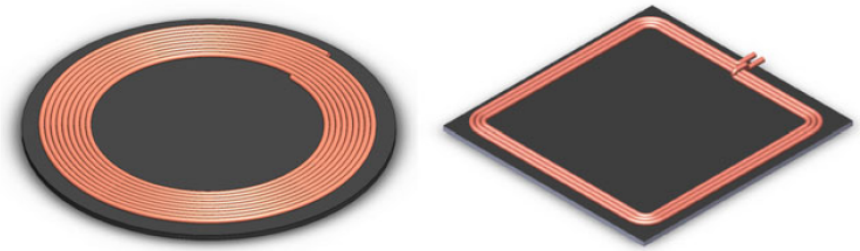

Fig. 5.4: Circular and rectangular coil without pitch

by

$$Number\ of\ strands = \frac{area\ of\ crossection\ of\ overall\ wire}{area\ of\ crossection\ of\ each\ strand} \tag{5.3}$$

In this work number of strands calculated is 2070.

(c) For deciding the construction of Litz wire, proximity and skin effect has to be considered. Simple twisting is adequate to eliminate the bundle level proximity effect but to avoid bundle level skin effect, multiple levels of twisting, also known as true Litz construction are required. First n_1 number of strands are twisted together, followed by twisting n_2 of those sub-bundles; additional stages are followed if required. The value of n_1 is given by

$$n_1 = \frac{4(skin\ depth)^2}{(diameter\ of\ single\ strand)^2} \tag{5.4}$$

It is calculated as 57.5. So first bundle turns should be less than that. So 57 is selected. Then for second and third level 3 is selected. For fourth level 4 is selected. So $57 \times 3 \times 3 \times 4$ will give approximately 2070 strands.

5.4.2 Design of pad geometry

Circular coils can be of 2 type with pitch and without pitch. For a circular coil of N turns without pitch, self inductance L is determined by the Eq 5.5

$$L = \mu_0 \times N^2 \times R \times \left(\ln \frac{16 \times R}{d} - \frac{7}{8}\right) \tag{5.5}$$

where μ_0 is the vaccum permeability, N is the number of turns, R is the radius of inner turn and d corresponds to the equivalent diameter of the coils.

$$d = 2 \times \sqrt{\frac{N \times S}{\pi}} \tag{5.6}$$

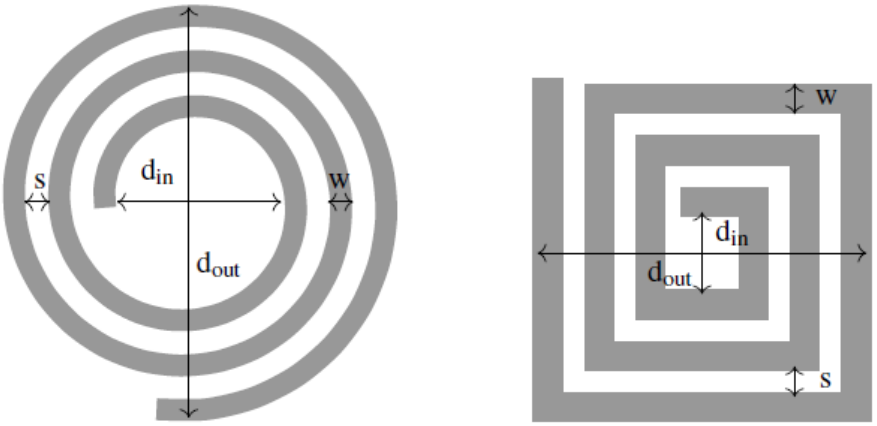

Fig. 5.5: Circular and rectangular coil with non-zero pitch

where S is the crossection of the wire.

R=10 cm is chosen, S is taken as the area of crossection of overall wire from Litz wire design. For L=218.6 μH, number of turns is calculated as 73.

If we are using a rectangular pad of dimension $a \times b$, Following equation is used to find the self inductance.

$$L = \mu_0 \times \pi \times N^2 \times [(a+b) \times \log(4 \times \frac{a \times b}{d}) - a \times \log(a + \sqrt{a^2+b^2}) \\ - b \times \log(b + \sqrt{a^2+b^2}) + 2 \times \sqrt{a^2+b^2} + (d - 2 \times (a+b))]$$

If we are using circular coil with non-zero pitch as shown in Fig.5.5. Then the inductance equation will be

$$L = \frac{\mu_0 N^2 d_{avg}}{2} \left(\ln \left(\frac{2.46}{\phi} + 0.2\phi^2 \right) \right) \tag{5.7}$$

where

$$d_{avg} = \frac{d_{out} + d_{in}}{2}$$

and

$$\phi = \frac{d_{out} - d_{in}}{d_{out} + d_{in}}$$

From Fig.5.5, d_{out} and d_{in} is related as.

$$d_{out} = d_{in} + 2W + (S + W)(2N - 1) \tag{5.8}$$

For rectangular coil with non-zero pitch , following equation has to be used.

$$L = 2.34\ \mu_0 \times \frac{N^2\ d_{avg}}{1 + 2.75\phi} \tag{5.9}$$

5.5 Conclusion

The various aspects affecting both self and mutual inductance is discussed. High frequency effects like proximity and skin effects are explained. Various pad topologies and their advantages are also discussed. A circular coil is designed and Litz wire requied for eliminating high frequency effects is also designed. Design equations for rectangular coil is provided.

CHAPTER 6

GSSA Modelling

6.1 Introduction

In order to obtain the relationship between the state variables inside the system, we need to derive the state space model of the system. While the general state space method is only applicable to linear systems, the wireless power transfer system is a kind of non-linear system due to the existence of switching devices and coupling resonant. Theoretically, the state space averaging model is used to analyze the state variables of the switching power supply system. The model requires that the system state variables have a slow time-varying characteristic compared to the switching frequency, while the WPT system with high frequency resonance has the similar frequency to switching devices within the system. As a consequence it cannot be applied in WPT system.

There emerges a generalized state space averaging method. The basic idea is to express the time domain periodic signal in the form of Fourier series. This method is suitable for resonance system and is an important method to analyze the internal characteristics of wireless power transmission system. Generalized averaging method is based on the fact that the waveform $x(\mathbf{.})$ can be approximated on the interval (t-T,t] to arbitrary accuracy with a Fourier series representation of the form

$$x(t-T+s) = \sum_{k} < x >_k \, e^{jkw_s(t-T+s)} \tag{6.1}$$

where the sum is over all integers k,$w_s = 2\pi/T, s \in (0,T]$ and the $< x >_k (t)$ are complex Fourier coefficients. These Fourier coefficients are functions of time since the interval under consideration slides as a function of time. The k'th coefficient or index-k

coefficient is given by

$$< x >_k (t) = \frac{1}{T} \int_0^T x(t - T + s) e^{-jkw_s(t-T+s)} ds \tag{6.2}$$

The analysis computes the time-evolution of these Fourier series coefficients as the window of length T slides over the actual waveform. Differentiation with respect to time property is given as

$$\frac{d}{dt} < x >_k (t) =< \frac{d}{dt} x >_k (t) - jkw_s < x >_k (t) \tag{6.3}$$

6.2 Modelling of DLCC topology

Fig 6.1 represents the generalized GSSA model of a WPT system. Losses in the inductors and capacitors are modelled with respective series resistances for getting accurate results. $R_{l1p}, R_{c2p}, R_{c2s}$ and R_{l1s} represents the losses in L_{1p}, C_{2p}, C_{2s} and L_{1s} respectively.

In addition, an existence function s(t) and a sign function sgn(x) can be useful in modelling the switching process of power electronic circuits. The existence function is defined in such a manner that it represents a train of square wave pulses with a magnitude of 1 or -1, while the sign function gives the sign of the input variable,i.e., the output is 1, 0, and -1 when the input is positive, zero, and negative respectively. Existence function which is used to model the inverter circuit is defined by

$$< s(t) >_n = \begin{cases} 0 & \text{n= 0,2,4....} \\ -\frac{2j}{n\pi} \sin\left(\frac{\beta}{2}\right) & \text{n= 1,3,5...} \end{cases} \tag{6.4}$$

In order to model the rectifier, sign function is used, as follows:

$$< sgn(x) >_1 = \frac{2}{\pi} e^{\angle < x >_1} \tag{6.5}$$

With this equations, the non-linear time-varying equations for the system states can be

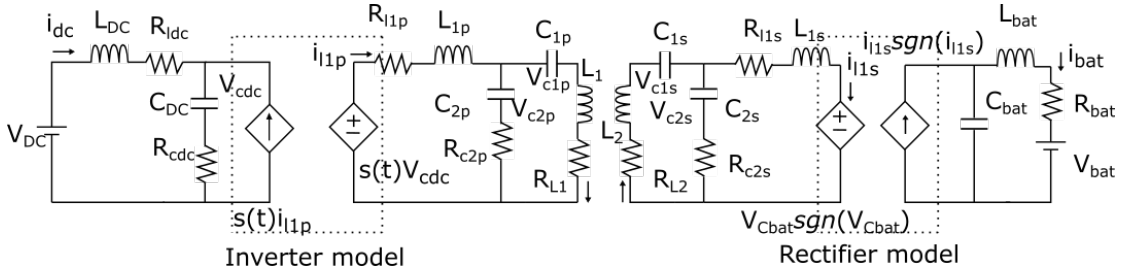

Fig. 6.1: GSSA Model of the system

written as follows:

$$
\begin{aligned}
L_{1p}\frac{di_{l1p}}{dt} &= s(t)V_{cdc} - V_{c2p} - R_{c2p}(i_{l1p} - I_1) - i_{l1p}R_{l1p} \\
L_1\frac{dI_1}{dt} &= R_{c2p}(i_{l1p} - I_1) + V_{c2p} - R_{l1}I_1 - V_{c1p} + M\frac{dI_2}{dt} \\
C_{2p}\frac{dV_{c2p}}{dt} &= i_{l1p} - I_1 \\
C_{1p}\frac{dV_{c1p}}{dt} &= I_1 \\
L_{1s}\frac{di_{l1s}}{dt} &= R_{c2s}(I_2 - i_{l1s}) - i_{l1s}R_{l1s} + V_{c2s} - V_{CB}sgn < V_{CB} > \\
L_2\frac{dI_2}{dt} &= -R_{c2s}(I_2 - i_{l1s}) - V_{c2s} - R_{l2}I_2 - Vc1s + M\frac{dI_1}{dt} \\
C_{2s}\frac{dV_{c2s}}{dt} &= I_2 - I_{l1s} \\
C_{1s}\frac{dV_{c1s}}{dt} &= I_2 \\
C_{dc}\frac{dV_{cdc}}{dt} &= I_{dc} + s(t)i_{l1p} \\
C_{bat}\frac{dV_{Cbat}}{dt} &= i_{l1s}sgn(i_{l1s}) - i_bat \\
L_{DC}\frac{di_{dc}}{dt} &= V_{DC} - V_{cdc} - (R_{cdc} + R_{ldc})i_{dc} \\
L_{bat}\frac{di_{bat}}{dt} &= V_{Cbat} - R_{bat}i_{bat} - V_{bat}
\end{aligned}
\tag{6.6}
$$

The state space equation is as follows

$$
\begin{aligned}
\dot{x} &= \mathbf{A}x + \mathbf{B}u(t) \\
y &= \mathbf{C}x + \mathbf{D}u(t)
\end{aligned}
\tag{6.7}
$$

Using GSSA and the following state variables, matrix A is obtained.

$$
\begin{aligned}
< i_{l1p} >_1 &= x_1 + jx_2 \\
< I_1 >_1 &= x_3 + jx_4 \\
< V_{c2p} >_1 &= x_5 + jx_6 \\
< V_{c1p} >_1 &= x_7 + jx_8 \\
< i_{l1s} >_1 &= x_9 + jx_{10} \\
< I_2 >_1 &= x_{11} + jx_{12} \\
< V_{c2s} >_1 &= x_{13} + jx_{14} \\
< V_{c1s} >_1 &= x_{15} + jx_{16} \\
< V_{cdc} >_0 &= x_{17} \\
< i_{dc} >_0 &= x_{18} \\
< V_{Cbat} >_0 &= x_{19} \\
< i_{bat} >_0 &= x_{20}
\end{aligned}
\tag{6.8}
$$

Applying Eqn 6.3 and deriving state space model.

$$
\begin{aligned}
A &= [A_1 \;\; A_2] \\
B[18,1] &= \frac{1}{L_{dc}}
\end{aligned}
\tag{6.9}
$$

All the other entries of B are zero.

$$
\begin{aligned}
C[1,20] &= 1 \\
D &= [0]
\end{aligned}
\tag{6.10}
$$

All other entries in C matrix are zero D=[0] This statespace equations are fed into MATLAB siso tool and transfer function for I_{bat} is found.

$$A_1 = \begin{bmatrix}
-\frac{r_1}{L_{1p}} & \omega & \frac{R_{p1}}{L_{1p}} & 0 & -\frac{1}{L_{1p}} & 0 & 0 & 0 & 0 & 0 \\
-\omega & -\frac{r_1}{L_{1p}} & 0 & \frac{R_{p1}}{L_{1p}} & 0 & -\frac{1}{L_{1p}} & 0 & 0 & 0 & 0 \\
\frac{R_{2p}L_2}{det} & 0 & -\frac{r_2L_2}{det} & \omega & \frac{L_2}{det} & 0 & -\frac{L_2}{det} & 0 & \frac{MR_{2s}}{det} & 0 \\
0 & \frac{R_{2p}L_2}{det} & -\omega & -\frac{r_2L_2}{det} & 0 & \frac{L_2}{det} & 0 & -\frac{L_2}{det} & 0 & \frac{MR_{2s}}{det} \\
\frac{1}{C_{2p}} & 0 & -\frac{1}{C_{2p}} & 0 & 0 & \omega & 0 & 0 & 0 & 0 \\
0 & \frac{1}{C_{2p}} & 0 & -\frac{1}{C_{2p}} & -\omega & 0 & 0 & 0 & 0 & 0 \\
0 & 0 & \frac{1}{C_{1p}} & 0 & 0 & 0 & 0 & \omega & 0 & 0 \\
0 & 0 & 0 & \frac{1}{C_{1p}} & 0 & 0 & -\omega & 0 & 0 & 0 \\
0 & 0 & 0 & 0 & 0 & 0 & 0 & 0 & -\frac{r_4}{L_{1s}} & \omega \\
0 & 0 & 0 & 0 & 0 & 0 & 0 & 0 & \omega & -\frac{r_4}{L_{1s}} \\
\frac{MR_{2p}}{det} & 0 & -\frac{Mr_2}{det} & 0 & \frac{M}{det} & 0 & -\frac{M}{det} & 0 & \frac{R_{2s}L_1}{det} & 0 \\
0 & \frac{MR_{2p}}{det} & 0 & -\frac{Mr_2}{det} & 0 & \frac{M}{det} & 0 & -\frac{M}{det} & 0 & \frac{R_{2s}L_1}{det} \\
0 & 0 & 0 & 0 & 0 & 0 & 0 & 0 & -\frac{1}{C_{2s}} & 0 \\
0 & 0 & 0 & 0 & 0 & 0 & 0 & 0 & 0 & -\frac{1}{C_{2s}} \\
0 & 0 & 0 & 0 & 0 & 0 & 0 & 0 & 0 & 0 \\
0 & 0 & 0 & 0 & 0 & 0 & 0 & 0 & 0 & 0 \\
0 & \frac{k}{C_{dc}} & 0 & 0 & 0 & 0 & 0 & 0 & 0 & 0 \\
0 & 0 & 0 & 0 & 0 & 0 & 0 & 0 & 0 & 0 \\
0 & 0 & 0 & 0 & 0 & 0 & 0 & 0 & \frac{4/\pi}{C_B} & 0 \\
0 & 0 & 0 & 0 & 0 & 0 & 0 & 0 & 0 & 0
\end{bmatrix} \tag{6.11}$$

$$A_2 = \begin{bmatrix}
0 & 0 & 0 & 0 & 0 & 0 & 0 & 0 & 0 & 0 \\
0 & 0 & 0 & 0 & 0 & 0 & \frac{-k}{L_{1p}} & 0 & 0 & 0 \\
-\frac{Mr_3}{det} & 0 & -\frac{M}{det} & 0 & -\frac{M}{det} & 0 & 0 & 0 & 0 & 0 \\
0 & -\frac{Mr_3}{det} & 0 & -\frac{M}{det} & 0 & -\frac{M}{det} & 0 & 0 & 0 & 0 \\
0 & 0 & 0 & 0 & 0 & 0 & 0 & 0 & 0 & 0 \\
0 & 0 & 0 & 0 & 0 & 0 & 0 & 0 & 0 & 0 \\
0 & 0 & 0 & 0 & 0 & 0 & 0 & 0 & 0 & 0 \\
0 & 0 & 0 & 0 & 0 & 0 & 0 & 0 & 0 & 0 \\
\frac{R_{2s}}{L_{1s}} & 0 & \frac{1}{L_{1s}} & 0 & 0 & 0 & 0 & 0 & \frac{2/\pi}{L_{1s}} & 0 \\
0 & \frac{R_{2s}}{L_{1s}} & 0 & \frac{1}{L_{1s}} & 0 & 0 & 0 & 0 & 0 & 0 \\
-\frac{r_3 L_1}{det} & \omega & -\frac{L_1}{det} & 0 & -\frac{L_1}{det} & 0 & 0 & 0 & 0 & 0 \\
-\omega & -\frac{r_3 L_1}{det} & 0 & -\frac{L_1}{det} & 0 & -\frac{L_1}{det} & 0 & 0 & 0 & 0 \\
\frac{1}{C_{2s}} & 0 & 0 & \omega & 0 & 0 & 0 & 0 & 0 & 0 \\
0 & \frac{1}{C_{2s}} & -\omega & 0 & 0 & 0 & 0 & 0 & 0 & 0 \\
\frac{1}{C_{1s}} & 0 & 0 & 0 & 0 & \omega & 0 & 0 & 0 & 0 \\
0 & \frac{1}{C_{1s}} & 0 & 0 & -\omega & 0 & 0 & 0 & 0 & 0 \\
0 & 0 & 0 & 0 & 0 & 0 & 0 & \frac{1}{C_{dc}} & 0 & 0 \\
0 & 0 & 0 & 0 & 0 & 0 & -\frac{1}{L_{dc}} & -\frac{r_5}{L_{dc}} & 0 & 0 \\
0 & 0 & 0 & 0 & 0 & 0 & 0 & 0 & 0 & -\frac{1}{C_B} \\
0 & 0 & 0 & 0 & 0 & 0 & 0 & 0 & \frac{1}{L_B} & -\frac{R_{bat}}{L_{bat}}
\end{bmatrix} \tag{6.12}$$

where

$$\begin{gathered}
R_{c2p} + R_{l1p} = r_1 \;\; ; \;\; R_{c2p} + R_{L1} = r_2 \\
R_{c2s} + R_{L2} = r_3 \;\; ; \;\; R_{l1s} + R_{c2s} = r_4 \\
R_{Ldc} + R_{Cdc} = r_5 \;\; ; \;\; det = L_1 L_2 - M^2 \\
k = \frac{4}{\pi} \sin \frac{\beta}{2}
\end{gathered} \tag{6.13}$$

6.3 Conclusion

Generalised state space modelling technique is explained in detail. The various equations used in modelling is also given. State space model for DLCC IWPT system is derived. The transfer function is obtained using ss2tf tool in MATLAB. The obtained transfer function is of the order 20.

CHAPTER 7

Control strategy and Simulation

7.1 Introduction

The output voltage and current are the functions of coil parameters, load impedance and switching frequency. The internal resistance of battery increases highly when it shifts from CC to CV mode. Even though constant current and constant voltage is ensured in design, there will be slight changes due to change in frequency, Harmonic components and neglect of resistances in resonant components. For providing proper current and voltage during charging and for automatic shifting from CC to CV mode , proper control has to be designed.

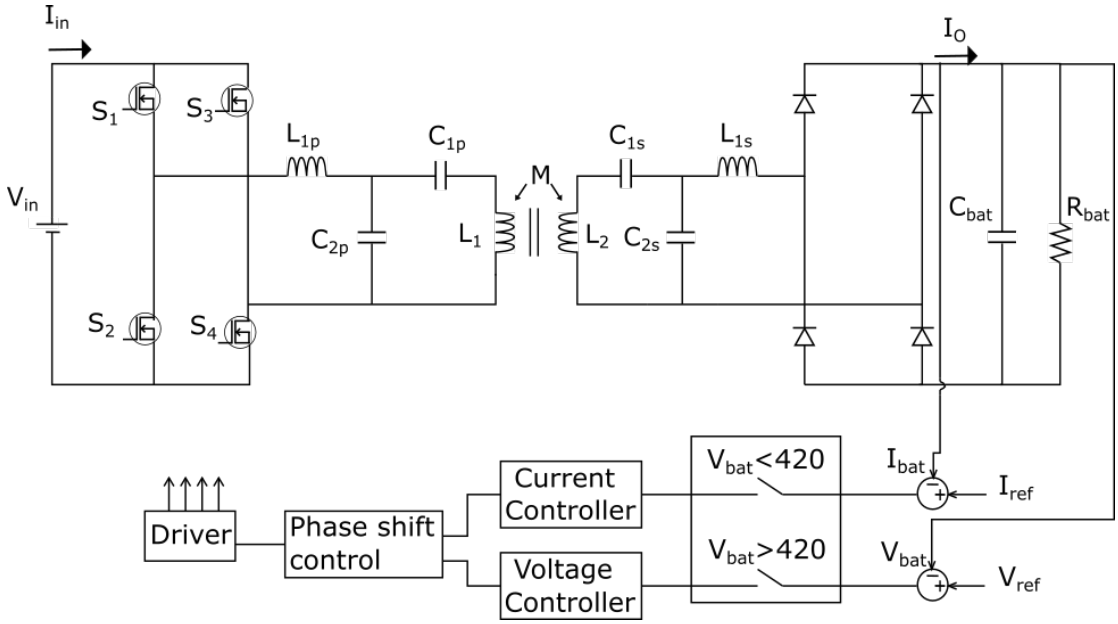

Fig. 7.1: Control of WPT

7.2 Control Methods

A wireless power transfer system can be controlled in different ways. Depending on where the control is applied, control methods can be classified as

(a) Primary control: In this mode, we can control the switching of inverter in the primary side.

(b) Secondary control: In this mode, we can control the secondary rectifier or we can have an extra DC-DC converter before battery to control power flow.

(c) Dual side control: In this mode, we will use combination of both primary and secondary control.

From one primary to one secondary pickup pad, generally we use primary side or dual side control. Secondary side control is used when multiple pickup pads are powered from one primary pad. The primary control need a wireless system which passes battery information from secondary to primary side. Secondary control needs one more stage in the charging system which increases cost and reduce reliability.

The control at primary side can be realised by changing the frequency, duty cycle or the phase shift between two legs. When frequency is adjusted, care should be taken to avoid bifurcation in loosely coupled systems. Also, frequency control method will need a wide frequency bandwidth which can probably increase the electromagnetic interference. For variable frequency methods, transfer efficiency and transformer size are hard to optimise. It can compensate reactive power, but a back-end converter will be required to regulate output current or voltage which will add an additional stage and hence increase cost and losses. In the case of fixed frequency, control can be either variation of duty cycle or phase shift. In these cases, there will be a high circulating current in the converter.

PWM control can compensate reactive power, but to control output current or voltage under varying load conditions such as a battery, wide duty ratio variation is needed which will increase switching loss since it deviate from Zero Voltage Switching (ZVS). In this work, phase shift control is implemented. Phase shift control is a method of controlling the output voltage by reducing the period of power transmission through the

phase difference between the leading leg and lagging leg of the primary side inverter. In this control, a delay of approximately half a resonant period is introduced from an update of conduction angle change in the H-bridge output voltage. Also conduction angle can only be updated twice per resonant period. The magnitude of H-bridge output voltage is controlled by conduction angle β. At steady state, the RMS value of the fundamental harmonic of V_{inv} can be expressed as

$$V_{inv} = \frac{4V_{dc}}{\sqrt{2}\pi} \sin(\frac{\beta}{2}) \tag{7.1}$$

where V_{dc} is the DC bus voltage. Note that relationship between V_{inv} and β is non-linear.

The LCC resonant tank acts as a band pass filter, passing only the fundamental harmonic of H-bridge voltage to the coils and all higher order harmonics will get trapped inside compensation network.

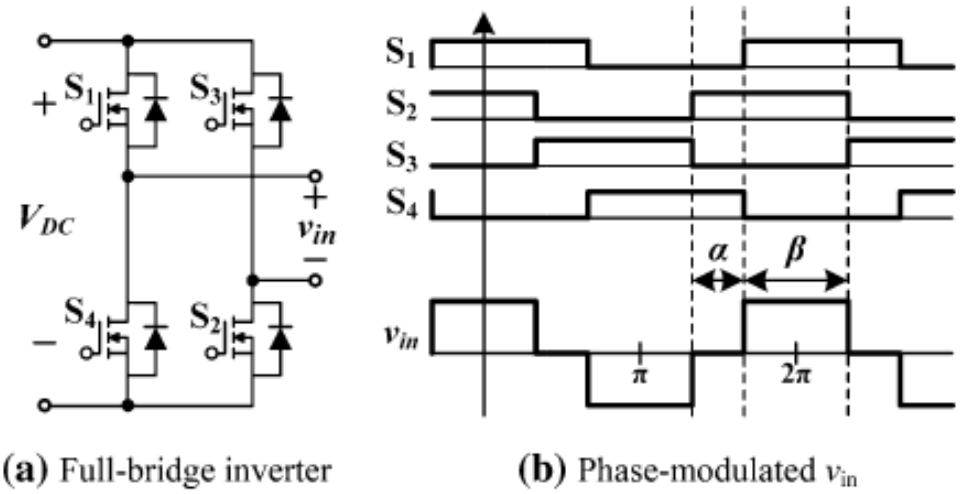

Fig. 7.2: Phase shift control

7.3 Control design

In this work, a closed loop control with a simple PI controller is adopted as shown in Fig 7.3. The controller is composed of a mode charge selection, a current controller, a voltage controller and a phase shift controller. Each of CC and CV mode charging requires

it's own independent controller, one of two is selected by mode selection according to the mode of charge. Mode selection is done by depending on battery voltage. If battery voltage is less than 420 V (which is maximum charge voltage), then current controller will be activated and CC charging will be enabled. At this time, voltage controller will be deactivated. Once battery charges and reaches 420 V, voltage controller will get activated and constant voltage charging will get enabled. At this time current controller will get deactivated. For designing PI controller, transfer functions of each mode is derived using GSSA modelling. The state space equations are given into MATLAB and required transfer functions are derived using MATLAB ss2tf tool and the required PI controller is designed using SISO tool in MATLAB.

The derived transfer function is of the order 20. So derivation in terms of parameters are difficult. So approximate values are fed into MATLAB and obtained transfer function is given in the previous chapter. where

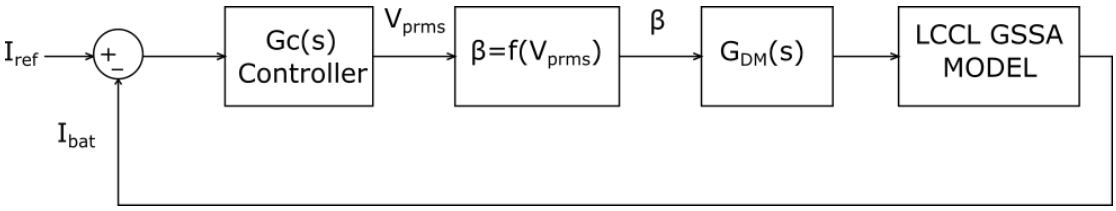

Fig. 7.3: Control block diagram for CC mode

$$G_{DM}(s) = \frac{\frac{2\sqrt{2}V_{dc}}{\pi}\sin(\frac{\beta}{2})}{\beta} \tag{7.2}$$

GSSA model is obtained from the previous chapter using ss2tf function. MATLAB siso tool is used to design the controller for the system. Controller $G_c(s)$ is designed for a bandwidth of 5×10^3 rad/s , phase margin of 69° and a gain margin of 20.1 dB. The frequency response plots are given in Fig 7.4.

$$G_c(s) = -5334.5 \times \frac{(1 + 0.00073s)(1 + 0.0017s)}{s(1 + 1.8e - 06s)} \tag{7.3}$$

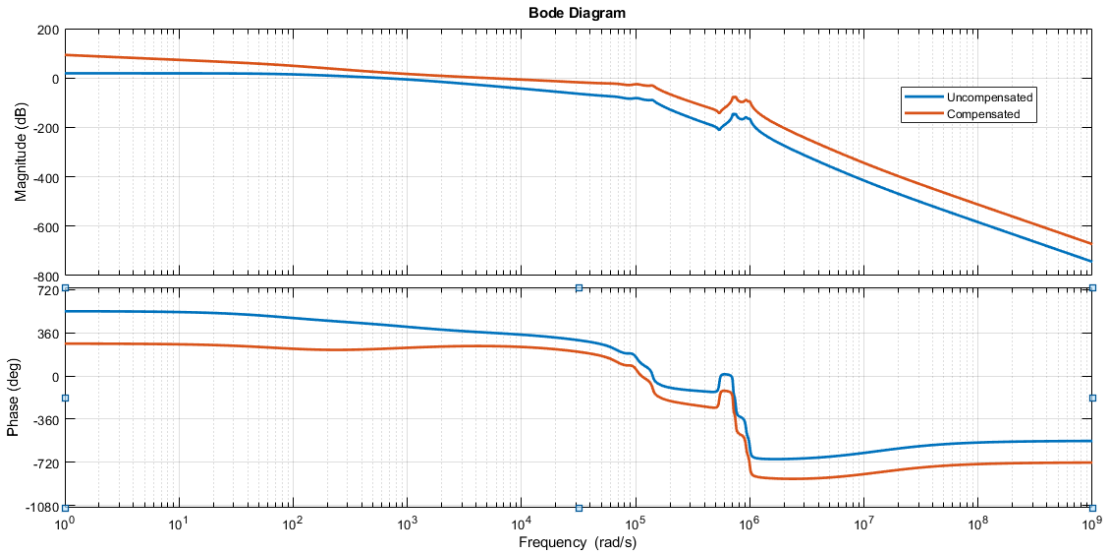

Fig. 7.4: Frequency response plot of Compensated and uncompensated loop of ICWPT control

7.4 Simulation results

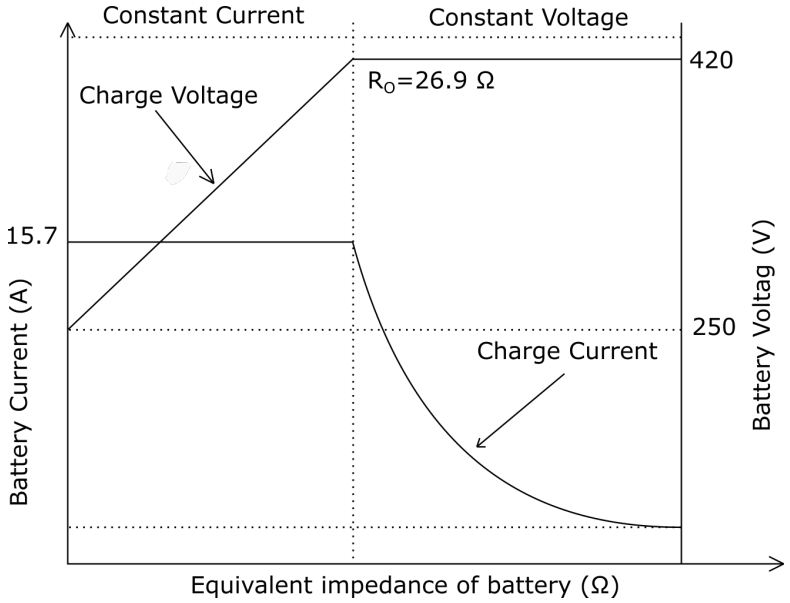

Fig. 7.5: CC-CV charge profile and equivalent impedance of battery

Battery is modelled as an RC load. The rated current in constant current mode is 15.7 A and the rated voltage in constant voltage mode is 420 V. The equivalent impedance at CC-CV mode transition is 26.9 Ω as shown in Fig. 7.5. So for representing Constant current mode, a load less than 26.9 is connected. The switches are operated in 68 KhZ. A step load change is given at 0.25 s. The simulation result is

given in Fig. 7.6. It can be observed that after the load change, the current remains constant and only the battery voltage changes.

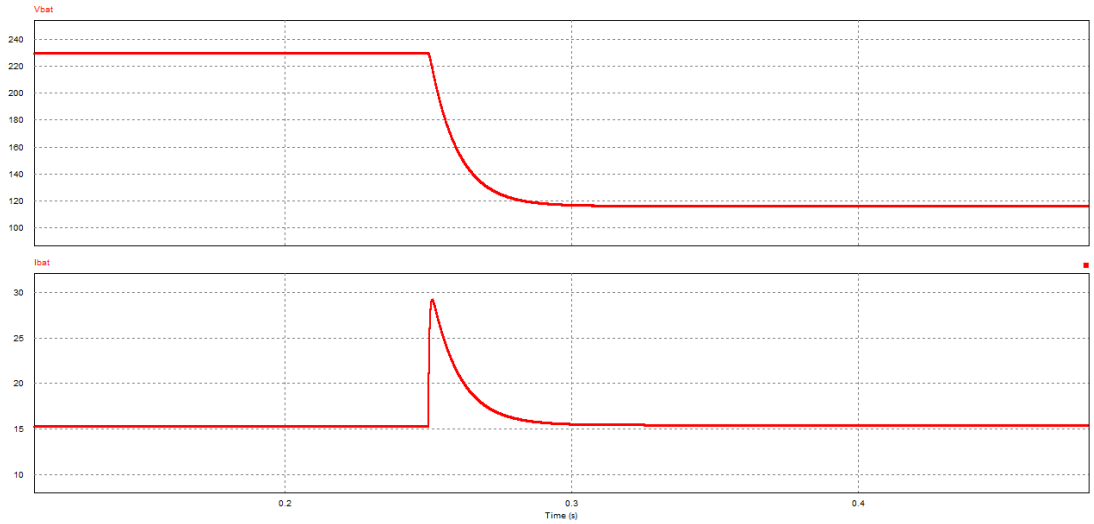

Fig. 7.6: Battery voltage V_{bat} and Battery current I_{bat} at CC mode

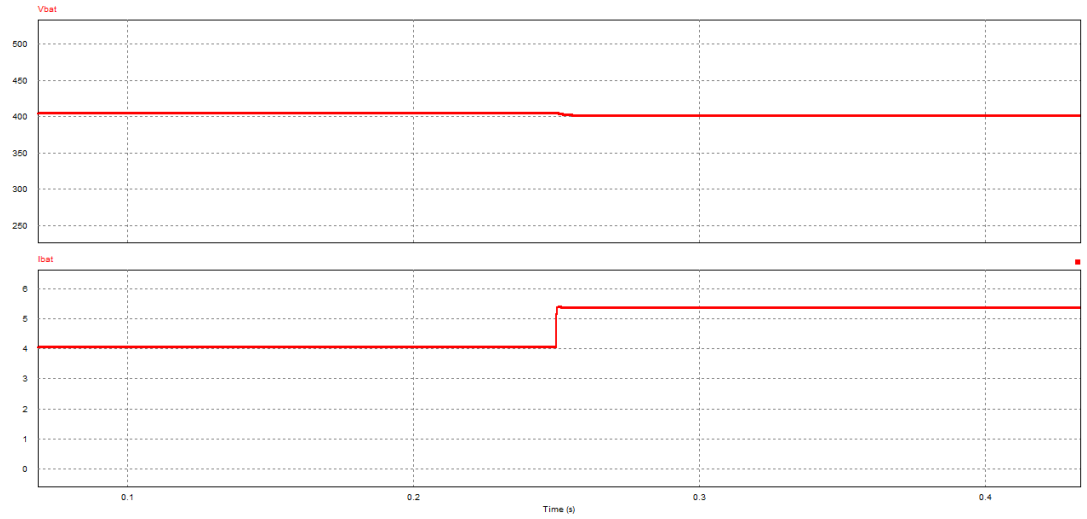

Fig. 7.7: Battery voltage V_{bat} and Battery current I_{bat} in CV mode

The constant voltage mode is represented with an RC load whose impedance is more than 26.9 Ω. The switches are operated in 78 kHz. A step load change is given at 0.25 s. The simulation result is given in Fig 7.7. It can be observed that, after the load change the output voltage remains constant where as output current changes.

Fig 7.8 shows the inverter output voltage and current in CC mode at 68 kHz. It is clear that Zero voltage switching (ZVS) and zero current switching is achieved as we designed for ZPA condition in CC mode. Fig 7.9 shows the inverter output voltage and

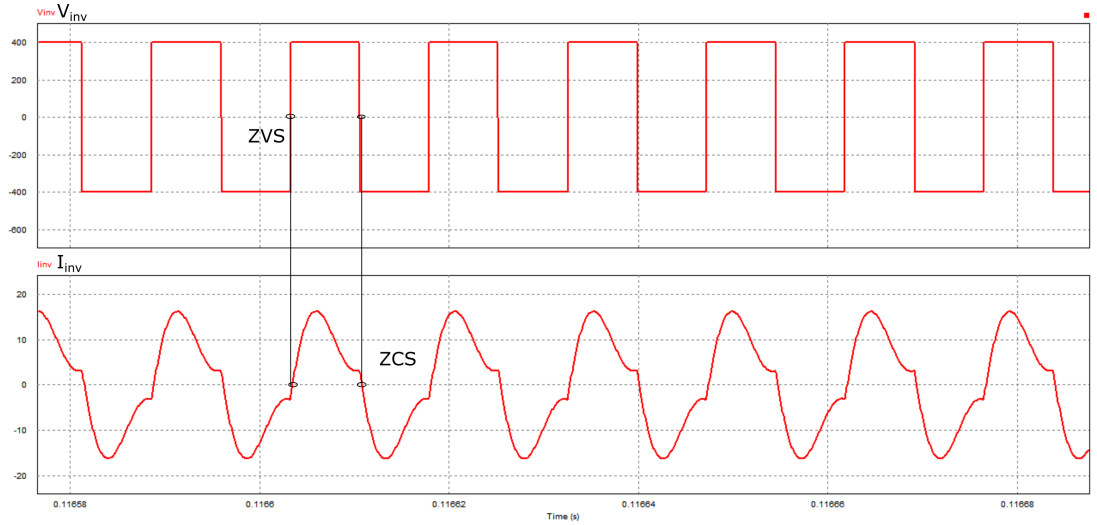

Fig. 7.8: Wave forms of V_{inv} and I_{inv} under CC mode

current in CV mode at 78 kHz. It can be observed that only ZVS is achieved and not ZCS.

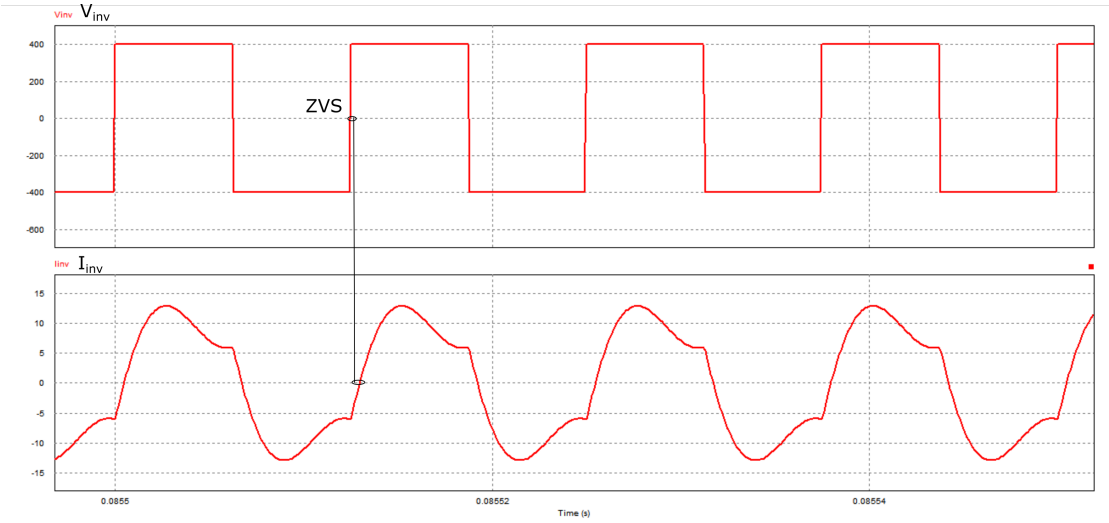

Fig. 7.9: Wave forms of V_{inv} and I_{inv} in CV mode

7.5 Conclusion

The various methods of controls are described. Phase shift control is implemented. The control strategy for the DLCC ICWPT system is discused. The simulation results at CC mode and CV mode are presented. Both modes gives constant output when load

changes. CC mode achieved both ZVS and ZVS where as CV mode achieved ZVS only.

CHAPTER 8

Conclusion and Future Scope

8.1 Conclusion

This thesis presents design and control strategy for an ICWPT system to achieve CC-CV charging of Li-ion battery. The proposed control strategy will automatically switch from constant current mode to constant voltage mode whenever the charging voltage is reached. The ICWPT is designed to operate in resonant frequency to reduce high Volt-Ampere rating. Also it ensures zero current switching and zero phase angle condition. The proposed method eliminates the use of additional back end dc-dc converter to achieve constant current and constant voltage modes. It also ensures minimum number of switches. The circular coil pad required for the ICWPT is designed analytically. The small signal model of DLCC compensated ICWPT system is presented and the required transfer functions are derived. Control strategy is presented and the controller design using frequency response analysis is discussed.

8.2 Future Scope

1. The design used a conventional circular pad for transmitter and receiver coil without ferrites. Other geometries can be used for lesser coil size, greater transfer distance and lesser copper material. Pads with ferrites also can be used which can be designed using FEM softwares.
2. The main drawback of ICWPT is the misalignment happening between transmitter and receiver coil. There are various compensation topologies and pad geometries which addresses this issue. Or proper control strategy should be used to reduce the effect of misalignment.
3. Dynamic wireless charging helps the EVs to get charged while moving which helps to have lesser battery size and long range. Stationary charging methods has to be extended to dynamic charging to avail this advantages. Vehicle dynamics and response time of control system have to be considered for this.

REFERENCES

[1] S. Hui, "Planar wireless charging technology for portable electronic products and qi," *Proceedings of the IEEE*, vol. 101, no. 6, pp. 1290–1301, 2013.

[2] D. Ahn and S. Hong, "Wireless power transmission with self-regulated output voltage for biomedical implant," *IEEE Transactions on Industrial Electronics*, vol. 61, no. 5, pp. 2225–2235, 2013.

[3] I.-G. Sîrbu and L. Mandache, "Comparative analysis of different topologies for wireless power transfer systems," in *2017 IEEE International Conference on Environment and Electrical Engineering and 2017 IEEE Industrial and Commercial Power Systems Europe (EEEIC/I&CPS Europe)*, pp. 1–6, IEEE, 2017.

[4] S. Li and C. C. Mi, "Wireless power transfer for electric vehicle applications," *IEEE journal of emerging and selected topics in power electronics*, vol. 3, no. 1, pp. 4–17, 2014.

[5] T. Kan, T.-D. Nguyen, J. C. White, R. K. Malhan, and C. C. Mi, "A new integration method for an electric vehicle wireless charging system using lcc compensation topology: analysis and design," *IEEE Transactions on power electronics*, vol. 32, no. 2, pp. 1638–1650, 2016.

[6] P. S. R. Nayak and D. Kishan, "Performance analysis of series/parallel and dual side lcc compensation topologies of inductive power transfer for ev battery charging system," *Frontiers in Energy*, vol. 14, no. 1, pp. 166–179, 2020.

[7] B. Esteban, M. Sid-Ahmed, and N. C. Kar, "A comparative study of power supply architectures in wireless ev charging systems," *IEEE Transactions on Power Electronics*, vol. 30, no. 11, pp. 6408–6422, 2015.

[8] J. Lu, G. Zhu, H. Wang, F. Lu, J. Jiang, and C. C. Mi, "Sensitivity analysis of inductive power transfer systems with voltage-fed compensation topologies," *IEEE Transactions on Vehicular Technology*, vol. 68, no. 5, pp. 4502–4513, 2019.

[9] C. Iclodean, B. Varga, N. Burnete, D. Cimerdean, and B. Jurchiş, "Comparison of different battery types for electric vehicles," in *IOP conference series: materials science and engineering*, vol. 252, p. 012058, IOP Publishing, 2017.

[10] V.-B. Vu, D.-H. Tran, and W. Choi, "Implementation of the constant current and constant voltage charge of inductive power transfer systems with the double-sided lcc compensation topology for electric vehicle battery charge applications," *IEEE Transactions on Power Electronics*, vol. 33, no. 9, pp. 7398–7410, 2017.